CORA Cork Open Research Archive
Cartlann Taighde Oscailte Chorcaí

Title	Motionless active depth from defocus system using smart optics for camera autofocus applications
Authors	Amin, M. Junaid;Riza, Nabeel A.
Publication date	2016-04-29
Original Citation	Amin, M. J. and Riza, N. A. (2016) 'Motionless active depth from defocus system using smart optics for camera autofocus applications', Proceedings of SPIE, 9896, Optics, Photonics and Digital Technologies for Imaging Applications IV, 98960N, SPIE Photonics Europe, 2016, Brussels, Belgium, 29 April. doi: 10.1117/12.2227753
Type of publication	Conference item
Link to publisher's version	10.1117/12.2227753
Rights	© 2016 Society of Photo-Optical Instrumentation Engineers (SPIE). One print or electronic copy may be made for personal use only. Systematic reproduction and distribution, duplication of any material in this paper for a fee or for commercial purposes, or modification of the content of the paper are prohibited.
Download date	2026-11-06 07:00:08
Item downloaded from	https://hdl.handle.net/10468/10107



UCC
University College Cork, Ireland
Coláiste na hOllscoile Corcaigh

PROCEEDINGS OF SPIE

SPIEDigitalLibrary.org/conference-proceedings-of-spie

Motionless active depth from defocus system using smart optics for camera autofocus applications

Amin, M. Junaid, Riza, Nabeel

M. Junaid Amin, Nabeel A. Riza, "Motionless active depth from defocus system using smart optics for camera autofocus applications," Proc. SPIE 9896, Optics, Photonics and Digital Technologies for Imaging Applications IV, 98960N (29 April 2016); doi: 10.1117/12.2227753

SPIE.

Event: SPIE Photonics Europe, 2016, Brussels, Belgium

Downloaded From: https://www.spiedigitallibrary.org/conference-proceedings-of-spie on 13 May 2020 Terms of Use: https://www.spiedigitallibrary.org/terms-of-use

Motionless Active Depth from Defocus System using Smart Optics for Camera Autofocus Applications

M. Junaid Amin[a] and Nabeel A. Riza*[a]
[a]School of Engineering, University College Cork, College Road, Cork, Ireland
*Corresponding author: n.riza@ucc.ie

ABSTRACT

This paper describes a motionless active Depth from Defocus (DFD) system design suited for long working range camera autofocus applications. The design consists of an active illumination module that projects a scene illuminating coherent conditioned optical radiation pattern which maintains its sharpness over multiple axial distances allowing an increased DFD working distance range. The imager module of the system responsible for the actual DFD operation deploys an electronically controlled variable focus lens (ECVFL) as a smart optic to enable a motionless imager design capable of effective DFD operation. An experimental demonstration is conducted in the laboratory which compares the effectiveness of the coherent conditioned radiation module versus a conventional incoherent active light source, and demonstrates the applicability of the presented motionless DFD imager design. The fast response and no-moving-parts features of the DFD imager design are especially suited for camera scenarios where mechanical motion of lenses to achieve autofocus action is challenging, for example, in the tiny camera housings in smartphones and tablets. Applications for the proposed system include autofocus in modern day digital cameras.

Keywords: Depth from defocus, Computational Imaging, Coherent radiation.

1. INTRODUCTION

Autofocus is a desirable feature in modern digital cameras which allows automatic focusing of blurred or out of focus regions of an image. Alternatively, users having modern cameras exhibiting autofocus characteristics can selectively choose regions within an image they want the camera to be focused on. Autofocussing action occurs via the use of mechanical motors, such as stepper motors or ultrasonic motors [1-2], which physically re-position the camera lens system's location within the camera architecture with respect to the sensor. This hardware action changes the imaging condition of the system and allows a different axially located object to be imaged (in focus) on the sensor. One of the steps in the autofocus process is to acquire the distance or depth of the target. Once this depth value is known, the lens-sensor separation can be set accordingly using the imaging condition to acquire an in-focus image of the target. In passive autofocus systems, depth is acquired by processing the spatial frequency information or texture variation of the target viewed by the camera. Depth from Focus (DFF) and Depth from Defocus (DFD) [3-4] are widely studied topics in literature and have been used for autofocus applications. DFF involves acquiring multiple images of a target each having a different degree of focus which is achieved via variation of camera parameters such as the lens-sensor separation or the aperture diameter. These images are processed in software to identify the image exhibiting the most focus (or sharpness). Knowing the camera parameters used to acquire this particular image and all other images, the target depth can be computed. With this information, the camera is accordingly re-set to focus correctly on the target. DFD involves acquiring depth values of a target by acquiring just 2 images of it, having different degrees of defocus. The amount of defocus in these images is processed to evaluate the depth. DFD requires just 2 images and hence is computationally more feasible than DFF. Features such as having a single viewpoint (i.e., single camera view), no time-of-flight wideband camera, use of a single conventional lens and minimal processing make this technique suitable for deployment in modern cameras.

Already popular in Digital Single-lens Reflex (DSLR) cameras, the autofocus feature is more recently deployed in miniature cameras housed within smartphones and tablets [5]. Like the bigger DSLR counterparts, these tiny cameras harbour small sized mechanical motors which move the lenses inside the tiny spaces in these cameras as part of the autofocus procedure [6]. The small sized spatial volume available for these cameras poses a significant design challenge to camera manufacturers. The additional drawbacks of using mechanical motors such as their bulky size and positional accuracy pose undesired concerns to smartphone and tablet camera imaging system designers. Furthermore, motion of

Optics, Photonics and Digital Technologies for Imaging Applications IV, edited by Peter Schelkens, Touradj Ebrahimi, Gabriel Cristóbal, Frédéric Truchetet, Pasi Saarikko, Proc. of SPIE Vol. 9896, 98960N · © 2016 SPIE · CCC code: 0277-786X/16/$18 · doi: 10.1117/12.2227753

Downloaded From: https://www.spiedigitallibrary.org/conference-proceedings-of-spie on 13 May 2020
Terms of Use: https://www.spiedigitallibrary.org/terms-of-use

mechanically movable parts can cause wear and tear which ultimately impact the working lifetime of these cameras. It is desirable to have a motionless camera design capable of effective autofocusing without using any mechanical motion of any camera component. Such a camera design capable of autofocus operation is presented in this paper. The presented camera design deploys a motionless smart optic that is an Electronically Controlled Variable Focus Lens (ECVFL) which allows the use of the focal length as the varying camera parameter for DFD operations, eliminating the need for any moving part components in the camera design. This allows a much desired motionless imager design which will be described in detail shortly.

Another challenge in camera autofocus systems relates to the scene information available for efficient autofocus operations. For autofocus systems to work for a certain target object in the scene, there needs to be sufficient information available on the object, such as contrast or spatial frequency variation of colour or texture, for autofocus image processing algorithms to use. In weak textured scenarios, even the most complex autofocus algorithms cannot make up for the lack of target spatial frequency information available to process, and therefore do not give desirable performance.

In such cases, autofocus "assist lights" are deployed which help camera autofocus algorithms by (a) providing distance measurements, or (b) providing artificial texture in the scene. Distance sensors such as laser time of flight [7] and triangulation methods [8] have been used as assist lights to provide object distance measurements to support autofocus image processing, but these have drawbacks. Range time of flight sensors require expensive high bandwidth electronics to work effectively, especially in shorter distances as the time period between the sending and receiving of light pulse is very small and demanding to process. Triangulation methods require a transmitter receiver separation to work effectively over longer distance ranges which proves as a design obstacle for modern handheld devices. Other assist lights used in cameras are incoherent projectors or Light Emitting Diodes (LEDs) which illuminate the scene with a certain optical pattern acting as artificial texture. These light patterns which are projected using a projection lens, however, have a limited depth of field over which the projected pattern appears to be sharp. Therefore, such sources have a restricted working range over which target autofocus is achieved. This is illustrated in Fig. 1(a) in which a conventional projector, connected to a Personal Computer (PC), illuminates the scene with a rectangular light pattern. A scene viewing camera, capable of autofocus, views the scene comprising of Object Planes (OPs) OP_1, OP_2 and OP_3. The projector is set to focus at OP_2, where the focused region of the pattern is present as shown in Fig. 1(a). However, OP_1 and OP_3, which lie outside the depth of field of such a projector, see defocused patterns which are non-ideal from an autofocus image processing point-of-view. Therefore, deploying conventional projectors limits the working range of autofocus cameras.

Hardware and software solutions have been suggested to overcome this projection limitation. Hardware solutions involve using multiple projected patterns each having a different axially located focus point to extend the working range of in-focus patterns [9]. But these units have increased hardware complexity without significant gain since only a few axial depth regions will have sharp focus retaining patterns. Software solutions involve modelling and evaluating the projector illumination's defocus, and using the acquired information in the overall DFD computation process [10]. However, this increased software complexity struggles when the illuminating patterns become too blurred. Ideally, one desires a projection system, such as shown in Fig. 2 which projects an in-focus sharpness retaining pattern over the OPs without needing complex hardware or software architectures. In this paper, such a desired active illumination module is presented in this paper which uses the conditioning of a highly coherent laser beam to provide illuminating patterns

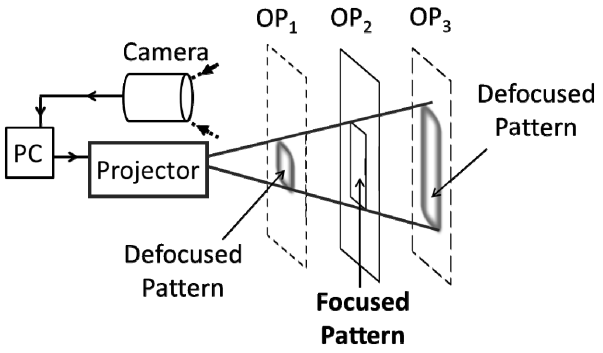


Fig. 1 (a) An active autofocus projection system is shown giving limited depth of field projection is shown. The illumination pattern is in-focus only at Object Plane OP_2.

Downloaded From: https://www.spiedigitallibrary.org/conference-proceedings-of-spie on 13 May 2020
Terms of Use: https://www.spiedigitallibrary.org/terms-of-use

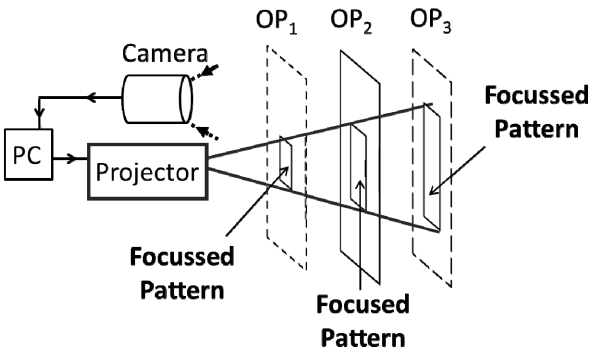


Fig. 2. A desired active autofocus projection system is shown giving a near-infinite depth of field projection is shown. The illumination pattern is in-focus at all OPs.

having near-infinite depth of field for most practical purposes. A complete motionless active DFD based system is described in the paper which overcomes the restricted working range of conventional active DFD systems as well as provides a no moving parts camera design for fast DFD operation. The rest of the paper describes the both modules (illumination and imager) of the motionless active DFD system in detail followed by a theoretical overview of DFD and an experimental demonstration showing the effectiveness of the presented design. The paper concludes with a summary of the key features of the system.

2. MOTIONLESS ACTIVE DEPTH FROM DEFOCUS SYSTEM USING SMART OPTICS

Presented in Fig. 3 is the motionless active DFD system design showing the illumination module and the imaging module. Both the modules are described next in detail.

2.1 Illumination Module

A detailed optical diagram of the illumination module is shown in Fig. 3. A coherent laser of wavelength λ passes through a Microscope objective onto a pinhole which projects an airy disc pattern towards a collimation lens located at a distance equal to its focal length. The resulting collimated laser beam passes through a programmable spatial filter optical mask which allows customization of the free-space propagating beam intensity profile. In Fig. 3, a square shaped mask is shown as an example which shapes the beam into a square shaped sharpness retaining beam. The mask can be programmed readily for any desired beam intensity profile, e.g., alternate regions of bright and dark stripes for

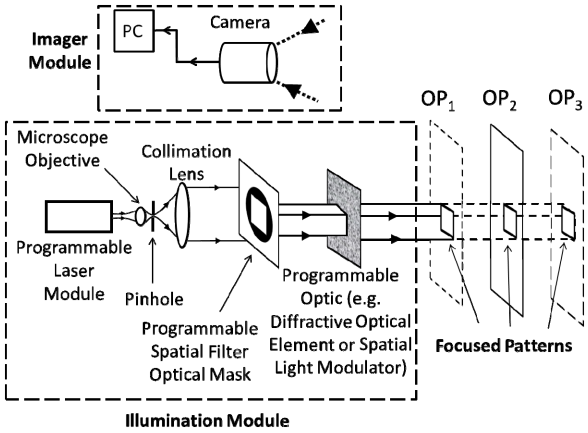


Fig. 3. Motionless active DFD system optical diagram showing (a) the illumination module giving sharpness retaining illuminating pattern over multiple axial distances, and (b) the imaging module responsible for the actual DFD operation.

Downloaded From: https://www.spiedigitallibrary.org/conference-proceedings-of-spie on 13 May 2020
Terms of Use: https://www.spiedigitallibrary.org/terms-of-use

applications requiring high spatial frequency variations. After the spatial filter optical mask, the beam passes through a programmable optic which could be, for example, a diffractive optical element, to project multiple sharpness retaining beams into diffraction orders to obtain coverage of a large field of view of the scene. A spatial light modulator as the programmable optic allow further conditioning reshaping, re-sizing or attenuation of the propagating beam depending on scene considerations. The conditioned beam then leaves the illuminating module and propagates towards the scene, retaining its sharpness owing to high coherence properties of laser beams.

2.2 Imager Module

The optical diagram of the motionless imager camera module which performs DFD operations is shown in Fig. 4. The design utilizes an ECVFL as part of the lens system of the camera. Scattered light from the scene enters the ECVFL and

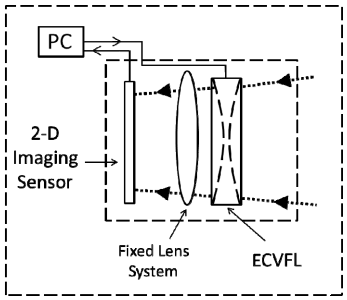


Fig. 4. Imaging camera module showing the ECVFL deployment as part of the camera lens system.

a fixed lens system before striking a two dimensional (2-D) imaging sensor connected to the PC. The key design feature from the DFD operation point of view is the use of the focal length of the lens system as the varying camera parameter for acquiring defocused images rather than the conventional routine of mechanically moving the lens system with respect to the 2-D sensor or controlling the size of the aperture. This motionless variation of the focal length is empowered using the ECVFL. Note that the 2-D imaging sensor can be based on standard CCD or CMOS chip technology or can use the novel Digital-Micromirror-Device (DMD)-based suited for high contrast scenarios [11].

The next section describes the theoretical aspect of the DFD algorithm, which uses focal length as the varying parameter, suited for the presented system.

3. DFD ALGORITHM USING FOCAL LENGTH AS THE VARYING PARAMETER FOR MOTIONLESS IMAGER MODULE

Although most modern day cameras exhibit multiple lenses for imaging operations, a single lens imaging system is assumed in this section for simplicity. Fig. 5 illustrates an optical ray diagram for such a single lens system which shows

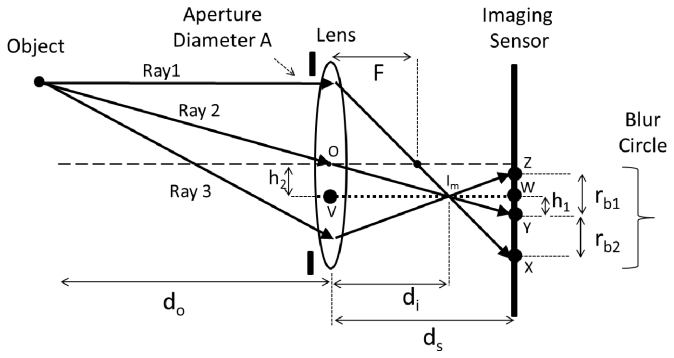


Fig. 5. Optical ray diagram of a single lens system illustrating the formation of the blur circle.

Downloaded From: https://www.spiedigitallibrary.org/conference-proceedings-of-spie on 13 May 2020
Terms of Use: https://www.spiedigitallibrary.org/terms-of-use

an object, a lens and an imaging sensor. In Fig. 5, d_o is the object-lens separation, F is the focal length of the lens, point O is the centre of the lens, h_2 is the vertical displacement below the optic axis to where the image point I_m is formed, point V is a distance of h_2 below point O, point W is the point on the imaging sensor which lies on the line connecting points V and I_m, point X on the imaging sensor is location where Ray1 strikes the sensor, point Y on the imaging sensor is location where Ray2 strikes the sensor, point Z on the imaging sensor is location where Ray3 strikes the sensor, h_1 is the separation between points W and Y, while r_{b1} and r_{b2} are the separations between points Y and Z, and Y and X, respectively. It can be seen in Fig. 5 that the imaging condition for the object is not fulfilled as d_i, the distance from the lens to the point where the image is formed, is different from the lens-sensor separation d_s. As a result, a so-called Blur Circle is formed on the imaging sensor having a diameter of the sum of r_{b1} and r_{b2}, as illustrated in Fig. 5. It can be shown that r_{b1} is equal to r_{b2} [12], therefore the radius r_b of the blur circle is given by:

$$r_b = \frac{A}{2}\left[\frac{d_s}{d_i} - 1\right] \quad . \tag{1}$$

The thin lens imaging equation is given by [13]:

$$\frac{1}{F} = \frac{1}{d_o} + \frac{1}{d_i} \quad . \tag{2}$$

Combining Eqns. (1) and (2) gives:

$$r_b = \frac{A}{2} d_s \left[\frac{1}{F} - \frac{1}{d_o} - \frac{1}{d_s}\right] \quad . \tag{3}$$

At this point, σ is defined as the blur parameter is written in terms of r_b as $\sigma = \mu r_b$, where μ is a constant depending on the optical properties of the system which needs to be experimentally calibrated. Eqn. (3) is re-written in terms of σ as:

$$\sigma_j = \mu \frac{A}{2} d_s \left[\frac{1}{F_j} - \frac{1}{d_o} - \frac{1}{d_s}\right], j = 1, 2 \, . \tag{4}$$

The subscript j is added to σ and F in Eqn. (4) since the two defocussed images acquired via the DFD system presented in this paper are taken using two focal length values, F_1 and F_2. These images will have two corresponding different values of σ (given by Eqn. (4)), σ_1 and σ_2, respectively. In order to relate σ_1 and σ_2 directly, d_o is made the subject of Eqn. (4):

$$d_o = \frac{1}{\frac{1}{F_j} - \frac{1}{d_s} - \frac{2\sigma_j}{\mu A d_s}}, j = 1, 2 \tag{5}$$

Eliminating d_o from the above equation results in an equation relating σ_1 and σ_2 and their respective focal lengths:

$$\sigma_1 - \sigma_2 = \frac{\mu A d_s}{2}\left[\frac{1}{F_1} - \frac{1}{F_2}\right] \quad . \tag{6}$$

This Eqn. (6) relation between the blur parameter and the focal lengths is of key significance. Next a relation between the blur parameter and the image content itself needs to be derived.

For this purpose, it is assumed that the Point Spread Function (PSF) *h* which describes the irradiance distribution at the imaging plane due to a point object follows a Gaussian profile given in terms of the blur parameter σ as [4]:

$$h(x, y) = \frac{1}{2\pi\sigma^2} \exp\left[-\frac{(x^2 + y^2)}{2\sigma^2}\right] \quad , \tag{7}$$

where x and y are spatial coordinates in the image plane. Let g(x, y) be a defocussed image acquired by the camera and f(x, y) be a focussed image acquired by the camera. g(x, y), f(x, y) and h(x, y) are related by:

Downloaded From: https://www.spiedigitallibrary.org/conference-proceedings-of-spie on 13 May 2020
Terms of Use: https://www.spiedigitallibrary.org/terms-of-use

$$g_j(x,y) = h_j(x,y) * f_j(x,y) \quad , j = 1,2. \tag{8}$$

Again the subscript j is added to signify two defocused images. In terms of Fourier Transforms (FTs), Eqn. (8) is written as:

$$G_j(u,v) = H_j(u,v)\, F_j(u,v) \quad , j = 1,2. \tag{9}$$

In Eqn. (9), G(u, v) is the FT of g(x, y), H(u, v) is the FT of h(x, y), F(u, v) is the FT of f(x, y) and u, v are the spatial frequencies in the x, y directions, respectively. The units u of and v are m^{-1}. Note that $f_1(x, y) = f_2(x, y)$ as both represent the focused image of the same scene, which also means $F_1(u, v) = F_2(u, v)$. Therefore eliminating F(u, v) from Eqn. (9) and rearranging gives:

$$\frac{G_1(u,v)}{G_2(u,v)} = \frac{H_1(u,v)}{H_2(u,v)}. \tag{10}$$

Note that H(u, v) is given by:

$$H(u,v) = \frac{1}{2\pi} \exp\left[-\sigma^2 \frac{(u^2 + v^2)}{2} \right] \quad . \tag{11}$$

Combining Eqns. (10) and (11) and using the logarithm, one gets:

$$\sigma_1^{\,2} - \sigma_2^{\,2} = -\frac{2}{(u^2 + v^2)} \log\left[\frac{G_1(u,v)}{G_2(u,v)} \right] \quad . \tag{12}$$

For each of the two images, the above equation expresses σ in terms of the frequency domain amplitude of a single point in the defocused image. From a computation point of view, it is more robust to use multiple points spanning a region R in the (u, v) domain of the defocused image. Therefore Eqn. (12) is re-written as an integral over a chosen region R:

$$\sigma_1^{\,2} - \sigma_2^{\,2} = -\frac{1}{\Omega_R} \iint_R \frac{2}{(u^2 + v^2)} \log\left[\frac{G_1(u,v)}{G_2(u,v)} \right] du\, dv, \tag{13}$$

where Ω_R is the area of R in the (u, v) space. Given two acquired defocused images using known camera parameters, Eqns. (6) and (13) are used to acquire values for σ_1 or σ_2. Once either σ is evaluated, Eqn. (5) is deployed to get the object depth. Fig. 6 summarizes the DFD algorithm steps. From a practical point of view, to acquire a depth map of the entire field of view, the image needs to be divided into sub-regions with each sub-region to undergo the described DFD process separately. Note that the algorithm described particularly Eqn. (6) is tailored for focal length as the varying camera parameter for acquired defocused images. For other varying camera parameters such as d_s, one needs to add the subscript j to d_s in Eqn. (4) and continue the derivation from there. This concludes an overview of the DFD process.

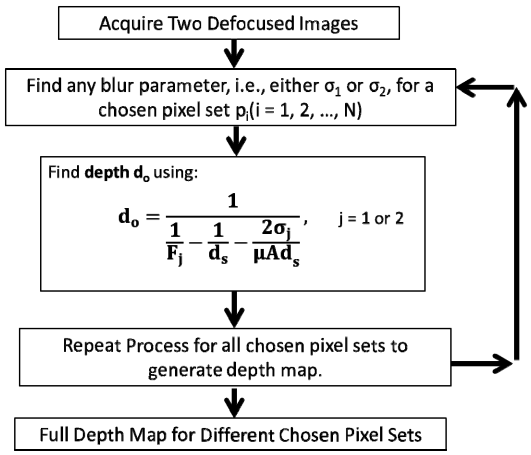


Fig. 6. Flow Diagram summarizing the steps of the DFD algorithm.

Downloaded From: https://www.spiedigitallibrary.org/conference-proceedings-of-spie on 13 May 2020
Terms of Use: https://www.spiedigitallibrary.org/terms-of-use

4. EXPERIMENTAL DEMONSTRATION OF THE MOTIONLESS ACTIVE DFD SYSTEM

Both the illumination and imaging modules of the presented motionless active DFD system are experimentally demonstrated. The components used in the experimental illumination module are: 15 mW He-Ne laser of $\lambda = 632.8$ nm deployed as a single wavelength source. Newport's MV-10X microscope objective having a numerical aperture of 0.25 and magnification of 10x is deployed, a 15 μm diameter pinhole, 40 cm focal length collimation lens located 40 cm from P, two rectangular cutouts of black page as spatial mask separated by 6.2 mm and each having dimensions of 18.9 mm (vertical) by 6.2 mm (horizontal). In the imaging module, the components used include an IDS CMOS sensor model no. UI-1250LE-M-GL having a pixel size of 5.3 μm and Optotune's 1 cm dimater EL-10-30 lens [14]. The target deployed is a planar black page covering the entire camera field of view at all axial locations along the experimental working range.

As comparison to the presented illumination module, the incoherent light source deployed a Philips LC4345 white light projector programmed to project rectangular stripes of similar dimensions to that of the illumination module's coherent

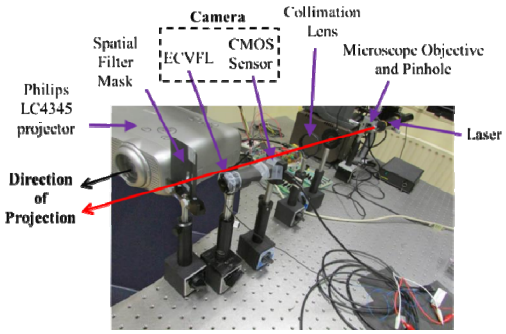
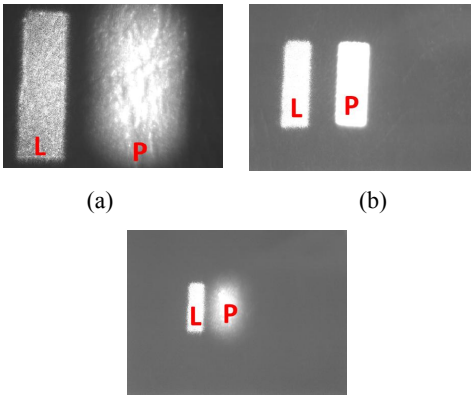


Fig. 7. Experimental setup showing the motionless active DFD system in operation.

conditioned pattern. The projector is pre-set to a best-focus distance of 56.8 cm with 12.5 cm of the projector's depth of field lying on the side closer to the system while 16.5 cm of the projector depth of field lies on the far-side. The experimental setup is shown in Fig. 7.

First, the illumination pattern of the presented coherent laser conditioning module is compared with that of the incoherent projector. For this, a working range of 30 cm to 100 cm is chosen for the experimental demonstration. The conditioned laser beam passes through only a single 18.9 mm (vertical) by 6.2 mm (horizontal) rectangular aperture, acting as the optical mask, before striking the black texture-less target while the conventional incoherent projector is programmed to project a single vertical rectangular stripe next to the laser illuminating stripe on the target. The laser stripe illuminating the target is labeled L while the projector stripe is labeled P. Fig. 8 shows the deployed camera



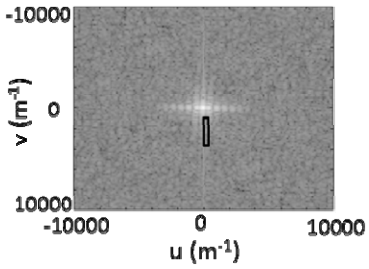
(a) (b)

(c)

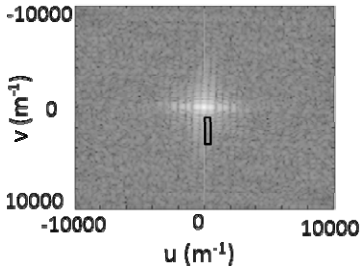
Fig. 8. Snapshots showing comparison of coherent conditioned laser illumination (stripe L) and incoherent white light projector (stripe P) for d_o values of (a) 31.0 cm, (b) 56.8 cm, and (c) 100.0 cm.

Downloaded From: https://www.spiedigitallibrary.org/conference-proceedings-of-spie on 13 May 2020
Terms of Use: https://www.spiedigitallibrary.org/terms-of-use

acquired in-focus snapshots of the stripe L (left) and stripe P (right), for d_o values of (a) 31 cm, (b) 56.8 cm which is the best-focus distance of the projector, and (c) 100 cm. Stripe P is blurred in Fig. 8(a) and (c) while it exhibits sharpness in Fig. 8(b). Stripe L, on the other hand, maintains its sharpness throughout the distance range. Now, a demonstration of the DFD algorithm in action is conducted. The first step involves calibrating the system to find the value of μ. Using two defocussed images acquired at d_o = 46 cm, μ is computed to be 2.74 $\times 10^5$ using the steps described in Section 4. Next, a complete distance measurement routine is carried out for both the illumination systems, i.e., the coherent conditioned beam and the incoherent projector, over the chosen working and range and the distance measurement data is compared. Sample images of the conditioned laser radiation only, with both mask rectangular stripes illuminated, are acquired using camera parameters of A = 1 cm and d_s = 9.8 cm. 2-D FTs of two sample defocused images, Image 1 (acquired by setting F_e to 9.30 cm) and Image 2 (acquired by setting F_e to 8.63 cm), acquired at d_o = 75.4 cm are computed using MATLAB's Fast Fourier Transform (FFT) function, and the zoomed version of the result is shown in Figs. 9(a) and (b), respectively. Note that an F_e = 8.81 cm allows a focused image to be captured for this d_o. From the Fig. 9 plots, it can be seen that Image 1 is more slightly more defocused given the relatively reduced spatial frequency amplitudes in Fig. 9(a) versus Fig. 9(b). The chosen region R is also highlighted in Figs. 9(a) and (b) illustrated a black rectangle.



(a)



(b)

Fig. 9. (a) zoomed 2-D FFT plot of defocused Image 1, and (b) zoomed 2-D FFT plot of defocused Image 2. Relevant parameters are: d_o = 75.4 cm, A = 1 cm, d_s = 9.8 cm, F_e for Image 1 = 9.30 cm, F_e for Image 2 = 9.30 cm and the F_e value for a focused is 8.81 cm.

A plot for the percentage error in depth measurement versus actual target depth acquired via DFD operations for both illumination projection techniques is illustrated in Fig. 10. In Fig. 10, the dots fitted by a black solid line represent data when deploying the coherent illumination module while the plus signs fitted with a dashed line represent data when the conventional incoherent projector is deployed. Note that the same DFD operation, i.e., the same motionless camera, is used to acquire two defocused images for each distance value measurement. The Fig. 10 data clearly shows an overall decreased percentage error in depth measurements when the coherent sharpness retaining illumination is deployed. This plot shows that a minimum in the percentage error curve occurs for the incoherent projector data set around the region where this projector exhibits its sharpest pattern and therefore, has most spatial frequency content on the target. Either

Downloaded From: https://www.spiedigitallibrary.org/conference-proceedings-of-spie on 13 May 2020
Terms of Use: https://www.spiedigitallibrary.org/terms-of-use

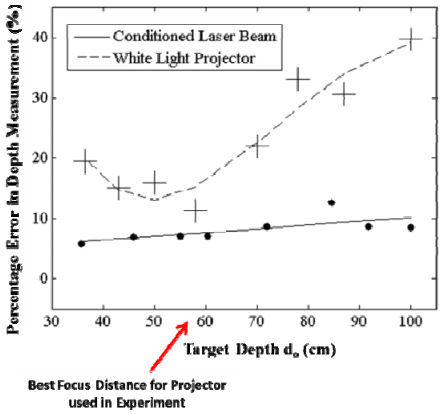


Fig. 10. Percentage error in DFD-based depth measurement and target depth d_o using conditioned coherent laser illumination (dots fitted by solid line) versus white light projector illumination (pluses fitted by dashed line).

side of this point, however, the incoherent projector's blurring of the illumination pattern increases the percentage error in depth estimation significantly as seen in Fig. 10. This problem is not present in the case of coherent conditioned illumination which projects a sharp pattern at all axial distances allowing the percentage error in distance measurements to be much less. For the coherent radiation, the percentage error stays within 10 % while for the incoherent illumination, the percentage error approaches 40 % towards the end of the chosen working distance range.

5. CONCLUSION

Presented is a motionless active DFD based system consisting of an illumination module which projects a coherent sharpness retaining pattern for enhanced DFD working range. A motionless imaging module is also described which allows DFD operations using focal length as the varying camera parameter. Theoretical basis of the deployed DFD algorithm is presented and an experimental demonstration is described which shows significant improvement in DFD based depth measurements by using the presented conditioned laser based illumination module as opposed to using a conventional incoherent projector. Applications include autofocus in weak textured scenarios. Full details of the system and its relevance to prior-art is described in ref. [15].

REFERENCES

[1] D. B Blackwell, G. A. Knaust, C. R Kropac, C. O Markkanen, J. M. Mccall, "Stepper motor control system," US Patent US3586953 A, 1971.
[2] Sashida, Toshiiku; Kenjo, Takashi, "Introduction to ultrasonic motors," Oxford Univ. Press, 1993.
[3] A. Pentland, "A New Sense for Depth of Field," IEEE Transactions on Pattern Analysis and Machine Intelligence, vol. PAMI-9, no.4, pp.523-531, (1987).
[4] M. Subbarao, "Parallel Depth Recovery by Changing Camera Parameters," Second International Conference on Computer Vision, pp.149-155, (1988).
[5] H. Jong-Woo, K. Jun-Hyung, L. Hyo-Tae and K. Sung-Jea, "A novel training based auto-focus for mobile-phone cameras," IEEE Transactions on Consumer Electronics, vol.57, no.1, pp.232-238, (2011).
[6] C.-S. Liu, P.-D. Lin, P.-H. Lin, S.-S. Ke, Y.-H. Chang and J.-B. Horng, "Design and Characterization of Miniature Auto-Focusing Voice Coil Motor Actuator for Cell Phone Camera Applications," IEEE Transactions on Magnetics, vol.45, no.1, pp.155-159, (2009).
[7] H. Surmann, K. Lingemann, A. N¨uchter and J. Hertzberg, "3D laser range finder for autonomous mobile robots," Proceedings of the 32nd ISR (International Symposium on Robotics), pp. 153 - 158, 19-21 April (2001).
[8] R. G. Dorsch, G. Häusler, J. M. Herrmann, "Laser triangulation: fundamental uncertainty in distance measurement," OSA Applied Optics, vol. 33, no. 7, pp. 1306-1314, (1994).

Downloaded From: https://www.spiedigitallibrary.org/conference-proceedings-of-spie on 13 May 2020
Terms of Use: https://www.spiedigitallibrary.org/terms-of-use

[9] H. Masuyama, H. Kawasaki and R. Furukawa, "Depth from Projector's Defocus Based on Multiple Focus Pattern Projection," IPSJ Transactions on Computer Vision and Applications 6, pp 88-92, (2014).
[10] L. Zhang and S. Nayar, "Projection defocus analysis for scene capture and image display," ACM Transactions on Graphics, vol. 25, no. 3, (2006).
[11] N. A. Riza, S. A. Reza and P. J. Marraccini, "Digital Micro-mirror Device-based broadband optical image sensor for robust imaging applications," Elsevier Optics Communications, vol. 284, no. 1, pp. 103-111 (2011).
[12] S. Chaudhuri, A. N. Rajagopalan and A. Pentland, "Depth From Defocus: A Real Aperture Imaging Approach," Springer, (1999).
[13] E. Hecht, "Optics," 4th Edition, Addison-Wesley, (2001).
[14] EL-10-30 datasheet, Optotune, Switzerland.
[15] M. J. Amin and N. A. Riza, "Active Depth from Defocus System using Coherent Illumination and a No Moving Parts Camera," Elsevier Optics Communications, (accepted paper), 2015.

Downloaded From: https://www.spiedigitallibrary.org/conference-proceedings-of-spie on 13 May 2020
Terms of Use: https://www.spiedigitallibrary.org/terms-of-use